Results in Physics 19 (2020) 103354

Contents lists available at ScienceDirect

Results in Physics

journal homepage: www.elsevier.com/locate/rinp

Construction of freeform mirrors for an off-axis telecentric scanning system through multiple surfaces expansion and mixing

Lu Chen[a], Zhishan Gao[a], Ningyan Xu[a], Xin Cao[a], Jianping Zhang[b], Lingjie Wang[b], Jingfei Ye[c], Qun Yuan[a,*]

[a] School of Electronic and Optical Engineering, Nanjing University of Science and Technology, Nanjing 210094, China
[b] Key Laboratory of Optical System Advanced Manufacturing Technology, Changchun Institute of Optics, Fine Mechanics and Physics, Chinese Academy of Sciences, Changchun 130033, China
[c] School of Physics and Optoelectronic Engineering, Nanjing University of Information Science and Technology, Nanjing 210044, China

ARTICLE INFO

Keywords:
Optical design
Scanning system
Off-axis telecentric
Freeform mirrors

ABSTRACT

In this paper, a direct design method for an off-axis two-mirror telecentric scanning system with a linear field of view (FOV) is proposed. A single freeform mirror structure is firstly considered, in which the aberration free geometry of the off-axis parabolic (OAP) surface is leveraged to provide the focusing function and build surface contour of the sub-region on the mirror for each FOV. Multiple OAP surfaces for construction of the freeform mirror are located at an OAP base to satisfy the telecentric condition. The imaging distortion of this single freeform mirror structure is analyzed and found unavoidable due to the unsymmetrical geometry of the OAP base. A freeform reflective corrector is supplemented, and it is constructed from multiple plane surfaces located at a curved base to fulfill the f-theta scanning geometry. Thus, a two-mirror structure composed of one freeform primary mirror and one freeform reflective corrector is established. Each plane-OAP surfaces pair corresponds to a specific FOV. These multiple OAP surfaces and multiple plane surfaces are then expanded and mixed respectively, to construct the freeform primary mirror and freeform reflective corrector. An f-theta two-mirror freeform scanning system with ± 10.4° linear FOV is designed using the proposed construction method. The design result is diffraction-limited, and a scanning error less than 5 μm and telecentricity angle less than 0.2° are achieved.

Introduction

Off-axis reflective systems have the advantages of having a compact structure, no central obscuration, a wide field of view (FOV), no chromatic aberration, and a high transmission [1]. As the rotational symmetry is broken when the system evolves from co-axial to off-axis, it is difficult to correct the aberrations induced by asymmetry using the traditional rotationally symmetrical spherical and aspherical surfaces [2]. A freeform optics is defined as an optics whose surface figure lacks rotational symmetry about the axis normal to the mean plane, and it offers more degrees of design freedom [3]. With the advancement of manufacture technologies in recent years, freeform optics have been widely used in imaging applications such as infrared imaging [4], space cameras [5], and remote sensing [6].

The strategies for designing freeform systems are of great importance [7]. The most common but brute-force design method is to vary all the coefficients that represent the figure of each freeform surface, and let the raytrace optimizer provided by the optical design software calculate the final coefficients and surface figures. However, this approach may lead to unintended consequences, and like-terms on multiple surfaces from the system may beat against each other, resulting in large freeform departure on each surface but with little optical performance gain. Therefore, creating an appropriate initial system is critical to achieve the optical requirements in an optimal manner. This is because the form of the optical system needs to be well constrained, with appropriate roles distributed at each surface. The final design results can be obtained by further optimization by utilizing the optical design software.

Many efforts have been made for direct design of a good starting point. Three major direct design methods have been proposed: the partial differential-equations method [8–10], the simultaneous multiple surface (SMS) method [11–12], and the construction-iteration method [13–15].The freeform surfaces are directly constructed based on object to image relations. For off-axis reflective systems design using the

* Corresponding author.
E-mail address: karmen86913@gmail.com (Q. Yuan).

https://doi.org/10.1016/j.rinp.2020.103354
Received 7 June 2020; Accepted 24 August 2020
Available online 09 September 2020

aforementioned methods, the initial system is usually set up with decentered and tilted planes or spherical mirrors for the elimination of obscuration [16]. However, the contours of these plane or spherical reference surfaces are far from that of freeform surface. This may affect the construction efficiency. We have paid more attention to the physical insight of the initial system, and proposed a construction method through multiple off-axis parabolic (OAP) surfaces expansion and mixing to design an easy-aligned freeform spectrometer [17]. A parabolic mirror is a specific aberration free component that focuses a collimated beam or collimates a divergent source perfectly, and its off-axis design allows the elimination of obscuration. The spherical surface of the collimating mirror in the spectrometer is replaced with an OAP surface, to obtain an aberration free geometry. The spherical sub-regions on the focusing mirror corresponding to the dispersed beams in the spectrometer are replaced with various OAP segments located at an OAP base, in order to obtain the aberration free geometry for each dispersed beam which can be considered as different FOVs. These multiple OAP surfaces are then expanded and mixed to construct a freeform surface integrating the collimating and focusing mirrors into a single element.

The construction method through multi OAP surfaces expansion and mixing is suitable for a single freeform mirror. In this paper, the characteristic of the OAP surface is studied comprehensively, e.g. the mapping distortion. Other than the previously utilized focusing function provided by the OAP segments for each FOV, as well as the telecentric condition satisfied by the OAP base, multiple plane surfaces are supplemented for mapping geometry fulfillment with low distortion. Moreover, the solution for the curved base to locate these multiple plane surfaces is a critical step. Thus, an OAP surface and a plane surface compose a plane-OAP surfaces pair corresponds to a single FOV. These multiple pairs are furtherly expanded and mixed to obtain two freeform mirrors. The proposed construction method are applied and elaborated in the design of an f-theta telecentric scanning system with a linear FOV using two freeform mirrors.

Characteristic analysis of OAP surfaces

Parameter definitions for the OAP mirror

Most imagers focus the object from infinity, in which a parabolic mirror forms a perfect image of a point for an axial object at infinity. Furthermore, a single OAP mirror might be the simplest optics that focuses a collimated beam or collimates a divergent source perfectly with an unobstructed optical path. Therefore, to fully leverage the characteristic of the OAP surface, it is adopted as a basic element for freeform mirror construction [17].

The optical layout of an OAP mirror that focuses a collimated beam with the aperture A is illustrated in Fig. 1, and our discussions are all restricted in the tangential plane. The chief ray of the collimated incident beam plotted as a bolded blue line traces along the central ray axis, that departs from the optical axis of the parent parabolic mirror, and the magnitude of departure is defined as decenter D. The OAP mirror is a side section of a parent parabolic mirror with this decenter D, and the focused beam is deviated by the off-axis angle β.

R represents the radius of the curvature of the parent parabolic mirror at the vertex, and f is the focal length of the parent parabolic mirror that equals to $R/2$. Therefore, the decenter D can be expressed as a function of R and β as shown below:

$$D = \frac{R(1-\cos\beta)}{\sin\beta} \tag{1}$$

Eq. (1) can also be transformed to calculate β as a function of D and R:

$$\beta = \operatorname{atan}\frac{D}{f-s} = \operatorname{atan}\frac{2RD}{R^2-D^2} \tag{2}$$

The off-axis sag s is defined as the sag for the center of the OAP mirror with respect to its vertex:

$$s = \frac{D^2}{2R} = \frac{D^2}{4f} \tag{3}$$

The reflected focal length $\hat{f}$ differs from the parent focal length f as:

$$\hat{f} = f + s = \frac{R}{2} + s \tag{4}$$

The reflected focal length $\hat{f}$ and the off-axis angle β are defined as a pair $(\hat{f}, \beta)$ to specify an OAP surface. The two marginal rays for the collimated beam are indicated as the top and bottom marginal rays, respectively as illustrated in Fig. 1.

Single mirror freeform structure evolved from multiple OAP surfaces

As a parabolic mirror only forms a perfect image of a point for an axial object at infinity, it can only provide good imaging performance within limited FOVs. Imagers such as the Newtonian telescope and the single reflective Head Mounted Display with a single curved mirror are the simplest structures [18]. The methodology for designing a single freeform mirror has been presented in our design works of the freeform focusing mirror in the spectrometer. The design schemes using multiple OAP surfaces are illustrated in Fig. 2.

The single freeform mirror imager provides the full linear FOVs of 2θ. According to the full aperture display of the imager in Fig. 2, the single mirror is ideally aberration free for each FOV. This means that each sub-region on the single mirror perfectly focuses the collimated beam for the specific FOV. Therefore, one OAP surface referred to as the OAP segment for each sub-region on the mirror for the corresponding FOV, is employed to fulfill the focusing function. This leads to the freeform mirror being a mixture of multiple OAP segments for the full FOVs.

In addition, the bottom illustration in Fig. 2 presents only the chief rays originated from the entrance pupil to the single mirror, and then the image plane. If the chief rays reflected from the single mirror are parallel, the telecentric condition is satisfied, and the imager will benefit a lot from this telecentric configuration. When considering only these chief rays, the optical layout of a perfect OAP surface referred to as the OAP base is configured. As each chief ray is reflected from the center of the corresponding OAP segment, it is easy to find that the centers of the OAP segments configure the contour of the OAP base. In other words, the OAP segments are located at the OAP base. The radius of curvature and the focal length of the OAP base are denoted as R_B and f_B.

As the linear FOV of the imager is $\pm\theta$, the top and bottom OAP segments located at the OAP base are for FOVs of $+\theta$ and $-\theta$ respectively. These are illustrated as the blue and violet bolded curves in Fig. 2. The pink bolded curve represents the OAP segment for FOV of 0°. Their off-axis angles at the distributed centers located at the OAP base are labeled as $\beta_{+\theta}$, $\beta_{-\theta}$ and β_0 respectively, and their decenter are $D_{+\theta}$, $D_{-\theta}$ and D_0. The image heights for FOVs of $+\theta$ and $-\theta$ are denoted as $H_{+\theta}$ and $H_{-\theta}$, and their signs differ.

Fig. 3 presents the details of the optical path as well as its specifications for the OAP segment for FOV of 0° which are colored in pink. The length of the chief ray from the entrance pupil to each OAP segment presents the reflected focal length at its corresponding center located at the OAP base, and that is denoted as $\hat{f}_{B0}$ for FOV of 0°. The length of the chief ray from each OAP segment to the image plane represents its reflective focal length, and that is denoted as $\hat{f}_{S0}$ for the OAP segment for FOV of 0°.

The off-axis angle β_0 is determined by the desired compactness and obstruction elimination for the single mirror imager. The parameters $\hat{f}_{B0}$ and $\hat{f}_{S0}$ are both restricted by the focal length of the imager. The vertex of the OAP segment for the FOV of 0° can easily be distinguished from

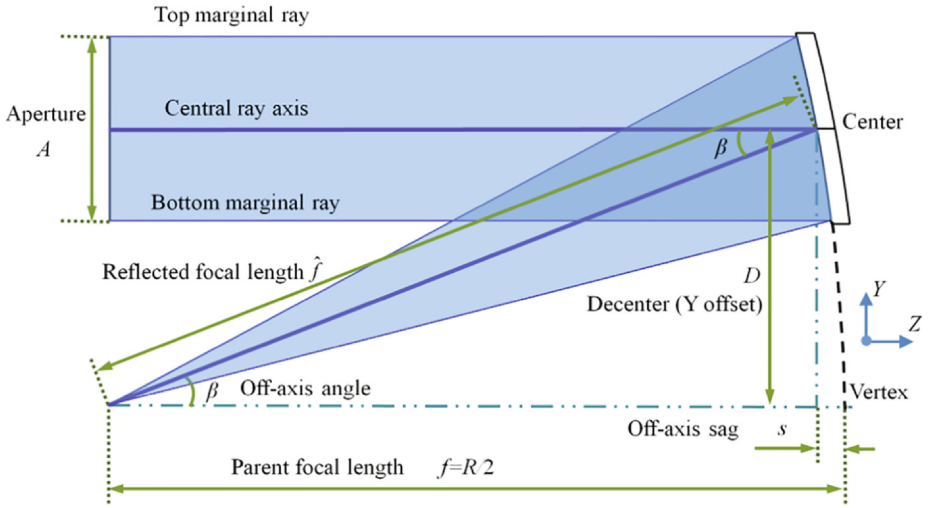

Fig. 1. Optical layout of the OAP mirror.

the vertex of the OAP base, and its decenter can be deduced from β_0 and $\hat{f}_{S0}$. Thus, the specifications for the OAP base are fully accomplished. The off-axis angles $\beta_{+\theta}$ and $\beta_{-\theta}$ for the OAP segment for FOVs of $+\theta$ and $-\theta$ can be deduced according to β_0 and the FOV. These are indicated by the simple geometrical relationship in Fig. 3 and expressed in the equation below:

$$\beta_0 = \beta_{+\theta} - \theta = \beta_{-\theta} + \theta \tag{5}$$

In the ideal inversed optical path from the image plane to the mirror, and then to the center of the entrance pupil, the chief rays are focused perfectly by the OAP base. Thus, the optical length of the chief ray from the entrance pupil to the image plane for any FOV is identical. In other words, the sum of its reflected focal length and the reflected focal length at its corresponding center located at the OAP base is constant for each OAP segment. Therefore, knowing the specifications of the OAP segment for FOV of 0°, as $\hat{f}_{B0}$ and $\hat{f}_{S0}$, the specifications of each OAP segment for any FOV can be deduced. In general, we have

$$\hat{f}_{B0} + \hat{f}_{S0} = \hat{f}_{B+\theta} + \hat{f}_{S+\theta} = \hat{f}_{B-\theta} + \hat{f}_{S-\theta} \tag{6}$$

where $\hat{f}_{B+\theta}$ and $\hat{f}_{B-\theta}$ signify the reflective focal length at the centers located at the OAP base for FOVs of $+\theta$ and $-\theta$ respectively, and $\hat{f}_{S+\theta}$ and $\hat{f}_{S-\theta}$ signify the reflective focal length of the OAP segment for FOVs of $+\theta$ and $-\theta$. These are not labeled in Fig. 3; however, it is easy to distinguish them according to their definitions. Therefore, the specifications for each OAP segment are determined.

Through the aforementioned calculations, the location of each OAP segment is determined with its center distributed at the OAP base. These OAP segments for the sampled FOVs are then mixed to form a freeform mirror. The measures for multi OAP surfaces expansion and

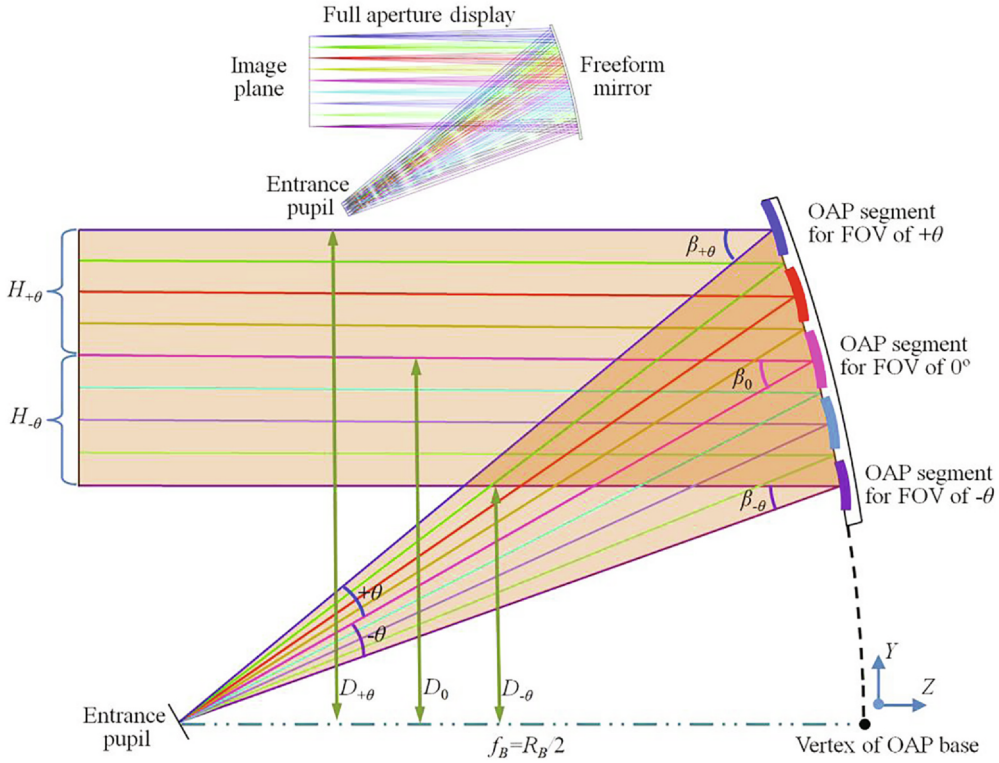

Fig. 2. Schemes for singe freeform mirror construction from multiple OAP surfaces.

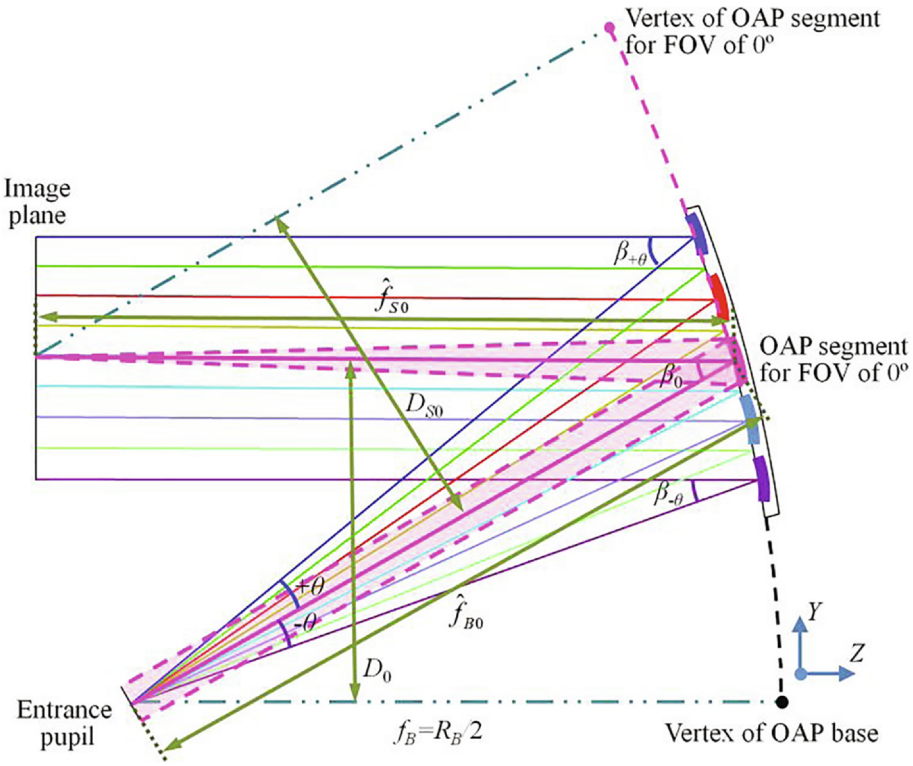

Fig. 3. Specification calculation scheme for the OAP segments.

mixing to construct a freeform mirror are the same as those described in Ref. [17], which will not be elaborated in this paper.

Imaging distortion of the single mirror freeform imager

Based on the construction method through multi OAP surface expansion and mixing, the focusing function and telecentric condition for the single mirror freeform imager are realized. Moreover, the imaging distortion is another key issue of an imager, so the mapping geometry of the construction method is studied.

As distortion is the aberration for chief rays, the mapping geometry of the bottom illustration in Fig. 2 is analyzed. Off-axis angle β_0 corresponds to the FOV of 0°, and $\beta_{+\theta}$ and $\beta_{-\theta}$ correspond to the FOVs of $+\theta$ and $-\theta$. These three chief rays are lines in pink, blue, and violet colors respectively in Fig. 2. Moreover, the chief rays for the FOVs of $+\theta$ and $-\theta$ are also the top and bottom marginal rays for the assumed collimated beams composed by the chief rays, as plotted in Fig. 1. As the chief ray for the FOV of 0° is the central axis, the image height for the FOV of $+\theta$ and $-\theta$ labeled as $H_{+\theta}$ and $H_{-\theta}$ are determined by the decenters $D_{+\theta}$, $D_{-\theta}$ and D_0. Their relationships are

$$D_0 = D_{+\theta} - H_{+\theta} = D_{-\theta} - H_{-\theta} \tag{7}$$

According to Eqs. (1) and (5), we have

$$D_0 = \frac{R_B(1-\cos\beta_0)}{\sin\beta_0} \tag{8}$$

$$D_{+\theta} = \frac{R_B(1-\cos\beta_{+\theta})}{\sin\beta_{+\theta}} = \frac{R_B[1-\cos(\beta_0+\theta)]}{\sin(\beta_0+\theta)} \tag{9}$$

$$D_{-\theta} = \frac{R_B(1-\cos\beta_{-\theta})}{\sin\beta_{-\theta}} = \frac{R_B[1-\cos(\beta_0-\theta)]}{\sin(\beta_0-\theta)} \tag{10}$$

The image height can be deduced and then simplified as

$$H_{+\theta} = D_{+\theta} - D_0 = \frac{2R_B}{\cot\frac{\theta}{2}(1+\cos\beta_0)-\sin\beta_0} \tag{11}$$

$$H_{-\theta} = D_{-\theta} - D_0 = \frac{-2R_B}{\cot\frac{\theta}{2}(1+\cos\beta_0)+\sin\beta_0} \tag{12}$$

Therefore, the image heights for FOVs of different signs are with both different signs and different absolute values. The difference is due to the unsymmetrical geometry of the OAP base which is its natural characteristic. As the OAP base is utilized to satisfy the telecentric condition, the imaging distortion for this single mirror freeform imager is unavoidable if the telecentric condition is fulfilled. In other words, the two requirements of telecentric condition and imaging distortion correction conflict in this single freeform mirror structure. Therefore, the evolvement of the freeform imager from single mirror structure to two-mirror structure is necessary to satisfy the telecentric condition and mapping geometry simultaneously.

Two-mirror telecentric scanning system construction

Design specifications for the f-theta telecentric scanning system

In order to elaborate the methodology for the construction of freeform mirrors in the off-axis system through multiple surfaces expansion and mixing, an f-theta telecentric scanning system is taken as an example. Usually, this system is built with lenses, and is ideal for use in optical coherence tomography, confocal laser scanning microscopy, and multiphoton imaging. The focusing spot size in the image plane is diffraction-limited and nearly constant over the full FOV, resulting in identical imaging resolution over the scanned area of the sample. The telecentric scan path can maximize the scattered or emitted light captured from the sample. A low f-theta distortion is a guarantee for the geometrically correct scanned images with no requirement of post-image processing. Therefore, the focusing function, telecentric condition, and f-theta scanning geometry are the three dominant issues for the scanning system. Design methods for scanning systems with a linear FOV using freeform optics have been proposed before by using a single lens, or two-mirror off-axis structure [19–20]. However, neither of them fulfills the telecentric condition.

Table 1
Specifications of the scanning systems.

Items	Scan lens (CLS-SL)	Off-axis two-mirror system
Wavelength range	400–750 nm	Broadband
Effective focal length	70 mm	70 mm
Entrance pupil diameter	4 mm	4 mm
Working distance	54 mm	44 mm
Scan angle (Single-axis scan)	± 10.4°	± 10.4°
f-theta distortion	< 5 μm	< 5 μm
Telecentricity	< 1.05°	< 0.2°

The scan lens CLS-SL vended by Thorlabs Inc. is taken as the reference for comparison, with its specifications listed in the second column of Table. 1. The scan lens could also provide square FOVs; however, the entrance pupil needs to be located between the two galvo mirrors for two-axis scan, and image quality is degraded. In this paper we would like to only consider single-axis scan. The scan lens is achromatic at visible wavelengths; nevertheless, an off-axis reflective system has no chromatic aberration. Thus, we make efforts to design an off-axis reflective scanning system having the same optical specifications, such as effective focal length, entrance pupil diameter, and the scan angle.

Construction of freeform corrector for distortion correction

The simplest structure with one freeform mirror is firstly studied according to the construction methodology described in Section 2.2. Off-axis angle β_0 is selected as 30° for obstruction elimination. The scan angle is ± 10.4°. Therefore, θ is 10.4°, $\beta_{+\theta}$ is 40.4°, and $\beta_{-\theta}$ is 19.6°. The reflected focal length $\hat{f}_{S0}$ for the OAP segment for FOV of 0° is 70 mm, which is equal to the effective focal length of the scanning system. The pair ($\hat{f}_{S0}$, β_0) used to specify the OAP segment for the FOV of 0° is determined. Deducing from the f-theta scanning geometry, the focal length, as well as the scan angle of ± 10.4°, the ideal image height denoted as h_θ is 12.706 mm for the maximum FOV of $+\theta$. The sum of the absolute values of the image heights for FOVs of $+\theta$ and $-\theta$ is constrained to be equal to twice the ideal image height for FOVs of $+\theta$, if the following equation is satisfied:

$$H_{+\theta} - H_{-\theta} = 2h_{+\theta} \tag{13}$$

According to Eqs. (11)–(13), R_B is deduced as 130.185 mm. D_0 and $\hat{f}_{B0}$ are derived as 34.883 mm and 69.766 mm respectively. Thus, the pair ($\hat{f}_{B0}$, β_0) used to specify the OAP base is determined. Thereafter, each OAP segment for the corresponding FOV or scan angle is then derived from the known specifications of the OAP base as ($\hat{f}_{B0}$, β_0), and the OAP segment for FOV of 0° as ($\hat{f}_{S0}$, β_0).

In this paper, the f-theta distortion is defined as the difference between the actual image height and the ideal image height. Assuming i is any specified scan angle between $+\theta$ and $-\theta$, the corresponding actual image height and ideal image height are denoted as H_i and h_i respectively. The f-theta distortion ΔH_i is then calculated as

$$\Delta H_i = H_i - h_i = H_i - \hat{f}_{S0} i \tag{14}$$

H_i is derived using the same strategy as $H_{+\theta}$ and $H_{-\theta}$ in Eqs. (11) and (12).

Deducing from the decenter values for each OAP segment, the f-theta distortion for the single mirror scanning system over the full FOV of ± 10.4° is plotted in Fig. 4. The f-theta distortion for FOVs from 0° to 1.4 ° is below zero, and their signs are all positive for other FOVs. In other words, the ideal chief ray incident on the image plane that fulfills the f-theta scanning geometry is mostly below the actual chief ray.

The mapping geometry differences are illustrated in Fig. 5(a), in which the ideal chief rays are plotted with dotted lines. Therefore, for distortion correction consideration, the directions of the chief rays should be bended to strike the image plane on the ideal locations. A

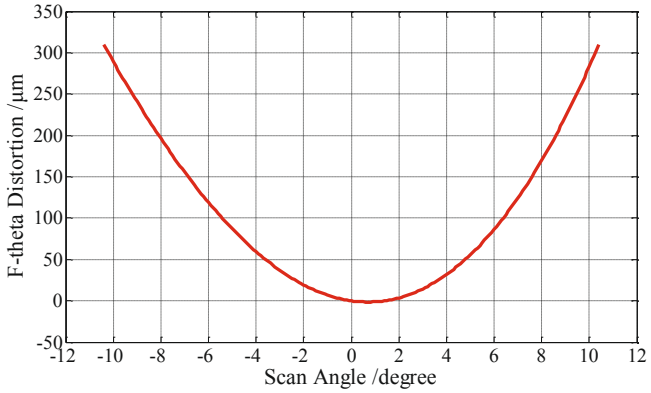

Fig. 4. F-theta distortion curve for the single mirror scanning system.

plane mirror is adopted in the Newtonian telescope for optical path folding. A folded plane mirror can then be utilized to bend the direction of the chief ray for one FOV, and it will not affect the focusing function provided by the freeform mirror. This freeform mirror evolved from multi OAP surfaces is referred to as the freeform primary mirror in this paper. One folded plane mirror corresponds to one specific OAP segment, and multi plane-OAP surfaces pairs are set up over the full FOV.

There are two positions to supplement these plane mirrors, one is between the entrance pupil and the freeform primary mirror, as illustrated in Fig. 5(b) for an unfolded optical path, and another is between the freeform primary mirror and the image plane, as illustrated in Fig. 5(c) for an unfolded optical path. These plane surfaces are then expanded and mixed to construct a freeform mirror. This is referred to as a freeform reflective corrector in this paper. Like the Schmidt corrector plate mainly for the correction of spherical aberration in a telescope, the dominant function of this freeform reflective corrector is for the correction of the specific aberration as distortion.

Thus, an off-axis two-mirror telecentric scanning system with a linear FOV is built. It is composed of one freeform primary mirror and one freeform reflective corrector. The possible geometries for the two-mirror scanning system are presented in Fig. 5(d) and (e), and are differentiated by the folding directions of the mirrors.

When the freeform reflective corrector is supplemented between the entrance pupil and the freeform primary mirror as illustrated in Fig. 5(b) and (d), the beam for each FOV is bended before incidence on the freeform primary mirror. Furthermore, the OAP segment for each FOV other than the FOV of 0° is updated. The off-axis angle $\beta_{+\theta}'$ for the updated OAP segment for the FOV of $+\theta$ is smaller than $\beta_{+\theta}$, and $\beta_{-\theta}'$ for the updated OAP segment for the FOV of -θ is also smaller than $\beta_{-\theta}$. This updated relationship between scan angles and off-axis angles provides mapping geometry without f-theta distortion. Moreover, the chief rays reflected by the updated OAP segments are still parallel, and the telecentric condition is maintained. These are illustrated in Fig. 5.

When the freeform reflective corrector is supplemented between the freeform primary mirror and the image plane as illustrated in Fig. 5(c) and (e), the beam for each FOV is bended after incidence on the freeform primary mirror. The OAP segment for each FOV remains the same. As the f-theta distortion differs over the full FOV as plotted in Fig. 4, the chief rays are bended by the freeform reflective corrector with different angles for distortion correction. Therefore, the previously parallel chief rays are non-parallel when they are bended, and the telecentric condition is broken. The telecentric condition and f-theta mapping conflict. Moreover, the working distance in configurations 3 and 4 is shorter than that in configurations 1 and 2.

Configuration 1 is then selected for the construction of the two-mirror scanning system, and the same methodology can be applied on configuration 2, with nearly the same optical performance accomplished ultimately. The optical layout of this two-mirror scanning system with multi plane-OAP surfaces pairs is illustrated in Fig. 6. The

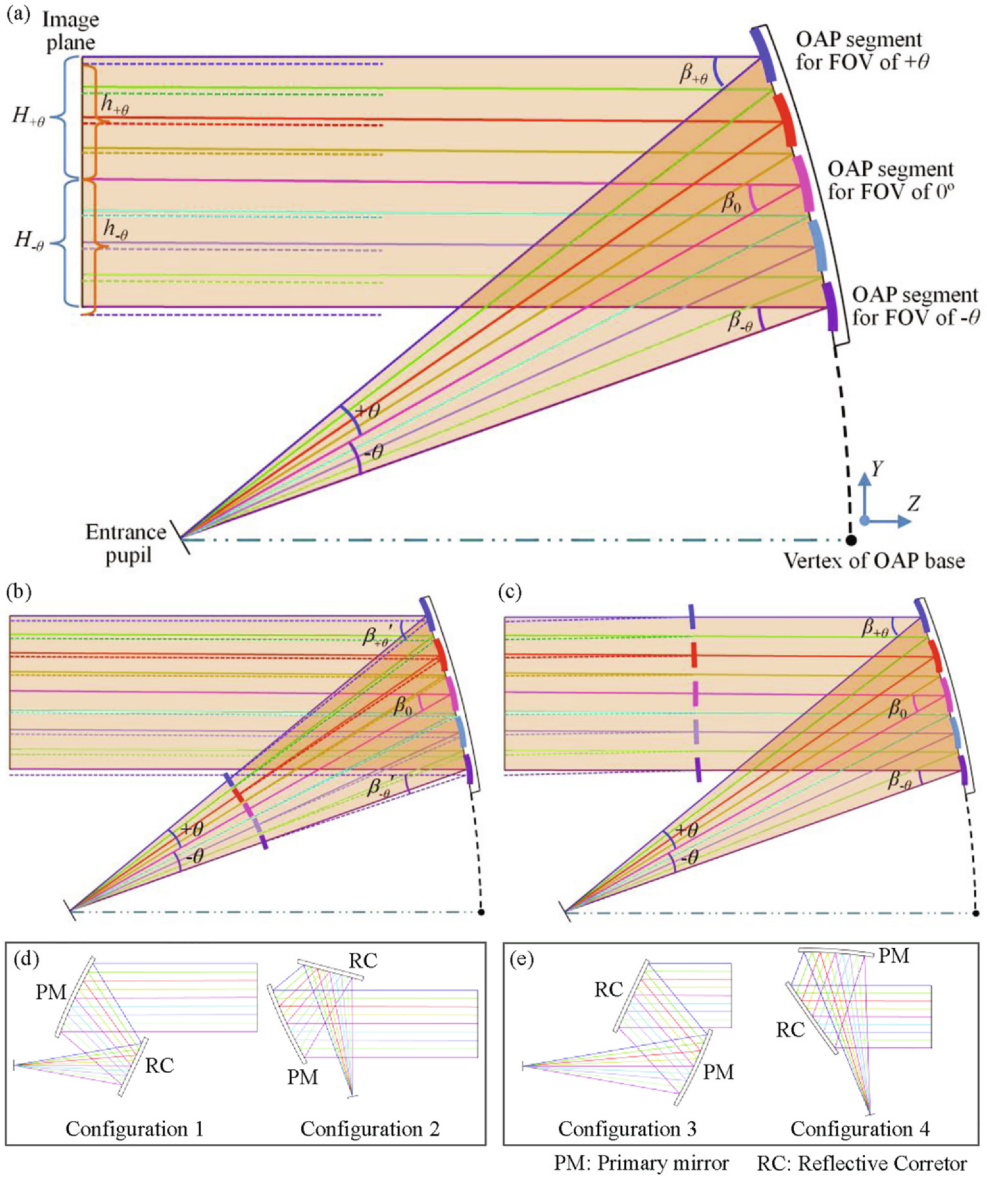

Fig. 5. Schemes for f-theta distortion correction. (a) Image height differences introduced by a single freeform mirror, (b) distortion correction through the supplement of multi plane mirrors between the entrance pupil and the freeform primary mirror for chief rays bending, (c) distortion correction through the supplement of multi plane mirrors between the freeform primary mirror and the image plane for chief rays bending, (d) possible geometries for the two-mirror scanning system corresponding to (b), (e) possible geometries for the two-mirror scanning system corresponding to (c).

off-axis angle β_0 is increased from 30° for single mirror structure to 50° for the placement of the two mirrors with obstruction eliminated. The freeform reflective corrector is tilted to let the chief ray for the FOV of 0° from the entrance pupil to be parallel to that incident on the image plane. The f-theta distortion over the full FOV of ± 10.4° induced by the freeform primary mirror is recalculated according to the reset off-axis angle of 50°. $\beta_{+\theta}$ is 60.4°, and $\beta_{-\theta}$ is 39.6°. $\hat{f}_{S0}$ is still 70 mm. R_B is recalculated as 114.473 mm. D_0 and $\hat{f}_{B0}$ are derived as 53.379 mm and 69.682 mm respectively. L_{CP} represents the optical length from the freeform reflective corrector to freeform primary mirror, and it is set as 32 mm for the elimination of obstruction, and then L_{EC} represents the optical length from the entrance pupil to the freeform reflective corrector, and it is 37.682 mm.

To correct distortion, the decenter value for the OAP segment is updated according to the ideal image height, and the corresponding off-axis angel β_i' is derived as:

$$\beta_i' = \operatorname{atan}\frac{2R_B(D_0 + h_i)}{R_B{}^2 - (D_0 + h_i)^2} \tag{15}$$

where $\beta_{+\theta}'$ and $\beta_{-\theta}'$ are calculated as 60° and 39.1° respectively. Thus, the previously established relationship between the FOV and the off-axis angle is updated, e.g. from $+\theta \rightarrow \beta_{+\theta}$ to $+\theta \rightarrow \beta_{+\theta}'$, from $-\theta \rightarrow \beta_{-\theta}$ to $-\theta \rightarrow \beta_{-\theta}'$. This update is accomplished by tilting each plane mirror for nonzero FOV with respect to that for the FOV of 0° to bend the chief rays. The tilt angle γ_i of the plane mirror for FOV of i is derived from the geometric relationship in Fig. 6.

$$\gamma_i = \frac{\beta_i' - \beta_0 - i}{2} \tag{16}$$

The tilted angle for each plane mirror is plotted as the curve representing the relationship between the scan angle and the tilted angle in Fig. 7.

These tilted plane mirrors are then mixed to construct the freeform reflective corrector. The direction of the beam for each FOV reflected by

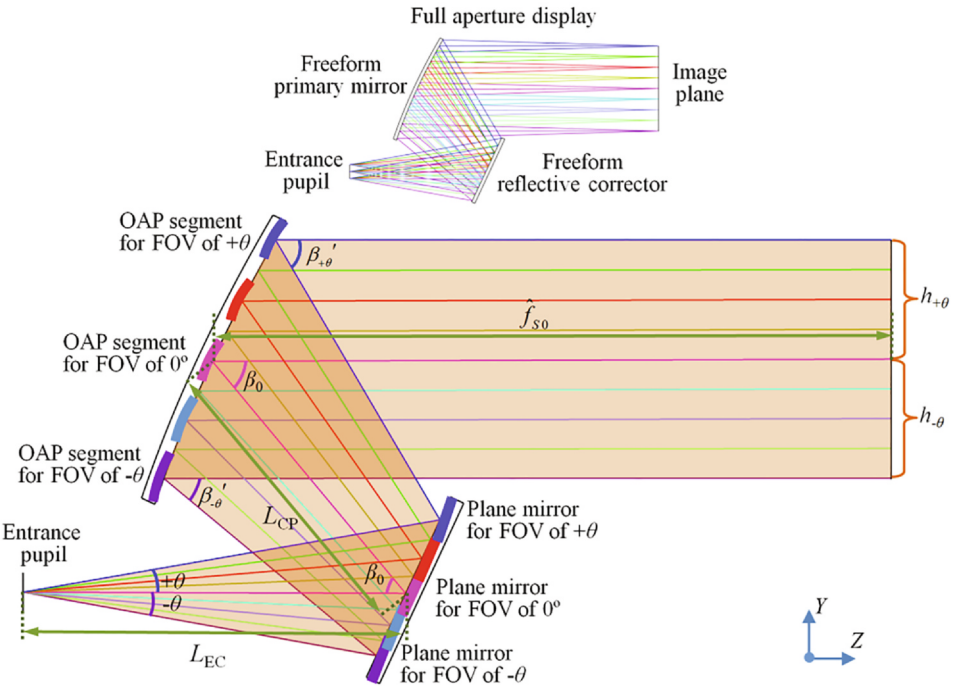

Fig. 6. Schemes for construction of two freeform mirrors in the scanning system from multiple plane-OAP surfaces pairs.

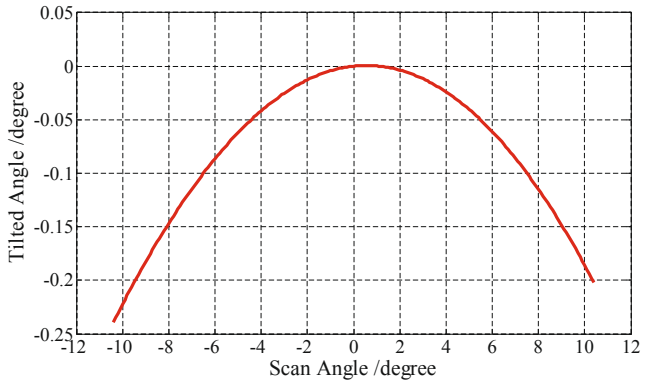

Fig. 7. Titled angle of the plane mirror for each FOV.

the corrector is determined by both its coordinates and normal vectors. Therefore, the discrete data points of the tilted plane mirrors are fitted to construct a freeform focusing mirror. However, if the centers of these tilted plane mirrors are located at a plane surface, the sags of the neighboring plane mirrors differ substantially because of the varying tilting angle for each FOV. The surface sag deviations in the overlapping areas cause worse mixing results.

An appropriate base is significant to avoid unphysical freeform corrector with discontinuous surface and slope. The schemes for the construction of a curved base are illustrated in Fig. 8. The FOVs are sampled with equal increment $\Delta\theta$ over the full FOV of $\pm\theta$. As presented in Fig. 8(a), $\Delta\theta$ in this paper is 0.1°. Therefore, we have 209 centers labeled as P_{-104} to P_{104}. These centers of the plane mirrors compose the curved base. The sag of the curved base is defined in the local coordinate system x-y-z. As L_{EC} is greatly larger than the sag of the curved base, this base is approximately as a plane surface for y coordinate calculation in Fig. 8(a). Assuming P_k is the center of the plane mirror for the FOV of $k\Delta\theta$, its y coordinate y_k can be easily derived in the triangle O-P_0-P_k, and we obtain

$$y_k = \frac{LEC\sin(k\Delta\theta)}{\sin(\alpha - k\Delta\theta)} = \frac{LEC\sin(k\Delta\theta)}{\sin(90^\circ - \frac{\beta 0}{2} - k\Delta\theta)} \tag{17}$$

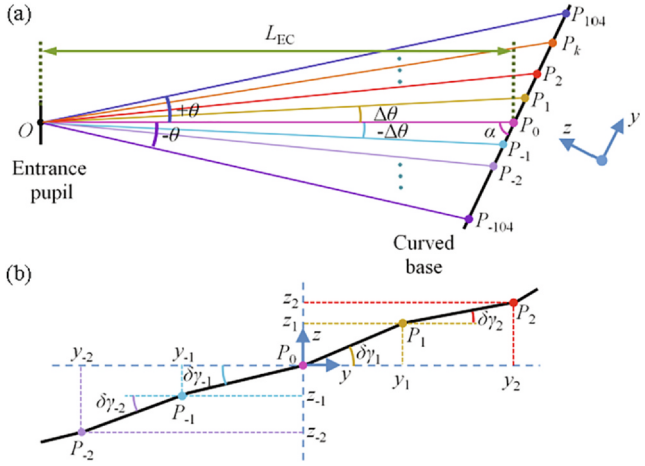

Fig. 8. Schemes for the construction of the curved base for multi plane mirrors. (a) Local y coordinates calculation. (b) Local z coordinates calculation.

Then its z coordinate can be derived in a step-by-step method from P_1, P_2, P_3…and P_{k-1} as presented in Fig. 8(b). We denote γ_k as the tilted angle for the plane mirror for the FOV of $k\Delta\theta$, and $\delta\gamma_k$ as the difference between the tilted angles for the neighboring plane mirrors, which is expressed as

$$\delta\gamma_k = \gamma_k - \gamma_{k-1} \tag{18}$$

The sag increment denoted as Δz_k for P_k with respect to P_{k-1} can then be deduced from the y coordinate increment and $\delta\gamma_k$.

$$\Delta z_k = \begin{cases} z_k - z_{k-1} = (y_k - y_{k-1})\tan\delta\gamma_k & (k > 0) \\ z_k - z_{k+1} = (y_k - y_{k+1})\tan\delta\gamma_k & (k < 0) \end{cases} \tag{19}$$

As P_0 is the origin of the local coordinate, z_1 equals Δz_1 is first derived, and then z_2, z_3…z_{103} and z_{104}, as well as z_{-1}, z_{-2}, z_{-3}…z_{-103} and z_{-104} are gradually calculated.

Therefore, the coordinates for the centers of the plane mirrors for the sampled FOVs are calculated. These are expanded from the center FOV to the marginal FOV. The profile of the curved base is plotted in

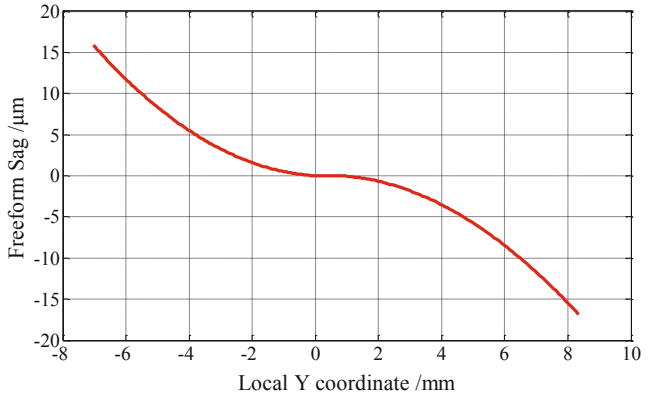

Fig. 9. Profile of the curved base.

Fig. 9. In other words, the locations of the plane mirrors for f-theta distortion correction are gradually constructed.

Considering feature rays from both different pupil sampling and multiple FOVs sampling, the coordinates and the normal of discrete points on each plane mirror are obtained with known the parameters of the curved base. These multiple plane surfaces located at the curved base are then mixed to construct the freeform reflective corrector, using both the coordinates and the normal of the discrete sampled points [21].

Construction result of the freeform two-mirror scanning system

The updated OAP segments are determined for f-theta distortion correction, and these multiple OAP surfaces located at the OAP base are then expanded and mixed to construct the freeform primary mirror. The construction method of the freeform reflective corrector and freeform primary mirror through multiple OAP and plane surfaces expansion and mixing is the same as that described for freeform spectrometer in Ref. [17]. Therefore, we will not elaborate it in this paper.

Thus, each plane-OAP surfaces pair corresponds to a single FOV, and composes the optical path for ideal focusing. The curved base for the plane mirrors, as well as the OAP base for the OAP segments provides the fulfillment of the f-theta scanning geometry and telecentric condition.

As the freeform reflective corrector that evolves from multi plane mirrors is implemented for distortion correction in the construction procedure, its freeform surface contours are constructed in the tangential plane. The surface sags for the constructed freeform reflective corrector and the freeform primary mirror are presented in Fig. 10. Both mirrors have a rectangular effective aperture, and XY polynomials up to fifth order are utilized to describe the surface sag. The XY polynomials terms such as y, y^2, y^3, y^4, and y^5 that are only in the tangential plane are used for the freeform reflective corrector.

The optical performance of the constructed freeform two-mirror scanning system is illustrated in Fig. 11. This is evaluated by the optical design software OpticStudio 16.5 SP2 (Zemax LLC, Kirkland, WA, USA) by importing the constructed parameters. The rms radius of the spot diagram for the sampled FOVs in Fig. 11(a) is around the airy radius of 11.7 μm at the working wavelength of 550 nm. The maximum f-theta distortion is larger than 10 μm over the full FOV as shown in Fig. 11(b), and telecentric condition is well fulfilled with constrained telecentricity angles less than 0.25°as shown in Fig. 11(c).

Further optimization and performance analysis

The constructed structure is taken as the benchmark, and a further optimization was performed leveraging the optical design software. The constructed surface contours for the freeform reflective corrector are in the tangential plane, and they only provide the function for distortion correction. Therefore, other XY terms that are symmetrical about the tangential plane are implemented and taken as variables. The optical length L_{EC} from the entrance pupil to the freeform reflective corrector is also variable with the initially calculated value of 37.682 mm.

The off-axis two-mirror telecentric scanning system with a linear FOV is finally achieved as shown in Fig. 12. The surface sags of the two freeform mirrors are illustrated in Fig. 13. They are close to the constructed surface sags presented in Fig. 10. L_{EC} is optimized to be 38.663 mm.

A diffraction-limited optical performance was accomplished through further optimization, as illustrated in Fig. 14(a). Other than the presented eleven sampled FOVs, spot diagrams over the full FOV are all diffraction-limited. These are checked and demonstrated by using the function of RMS spot radius vs field in the optical design software. The

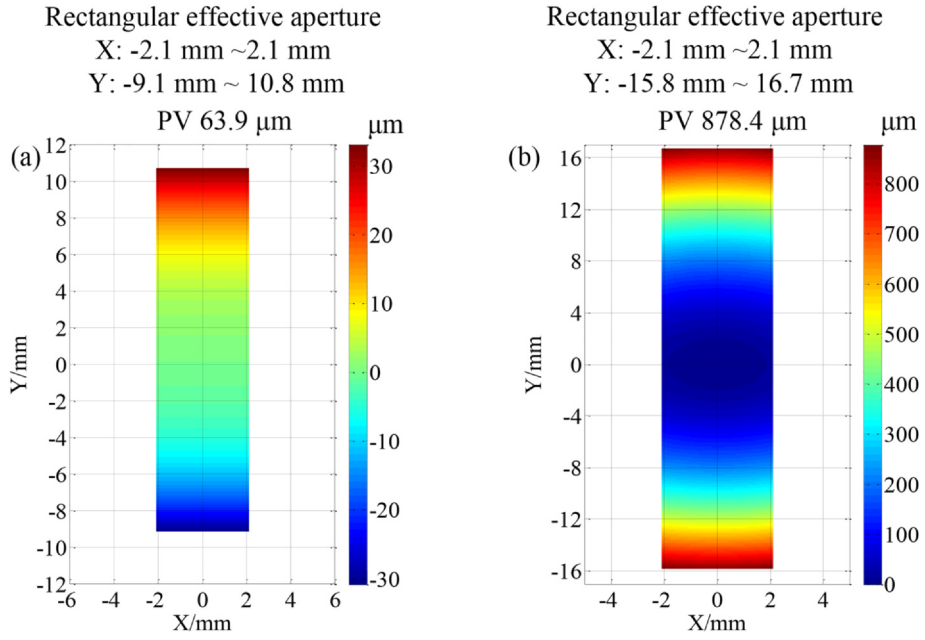

Fig. 10. Surface sag of the constructed freeform mirrors. (a) Reflective corrector, (b) primary mirror.

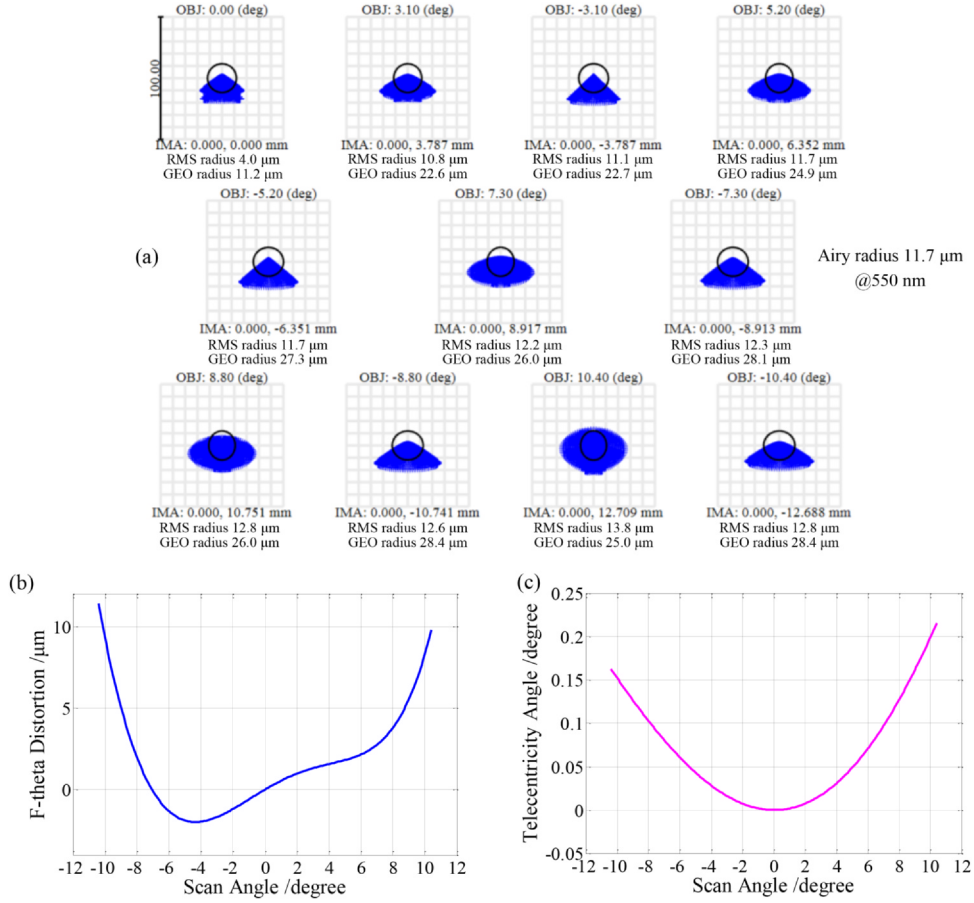

Fig. 11. Optical performance of the constructed freeform two-mirror scanning system. (a) Spot diagrams of the sampled FOVs on the image plane, (b) f-theta distortions and (c) telecentricity angles over the full FOV.

Fig. 11. Optical performance of the constructed freeform two-mirror scanning system. (a) Spot diagrams of the sampled FOVs on the image plane, (b) f-theta distortions and (c) telecentricity angles over the full FOV.

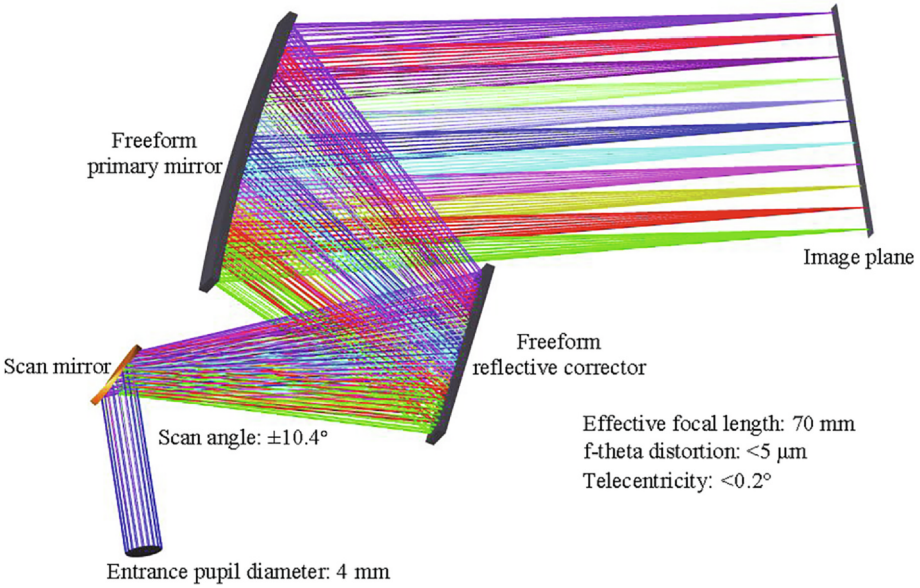

Fig. 12. The optical layout of the off-axis two-mirror telecentric scanning system using freeform mirrors with a linear FOV.

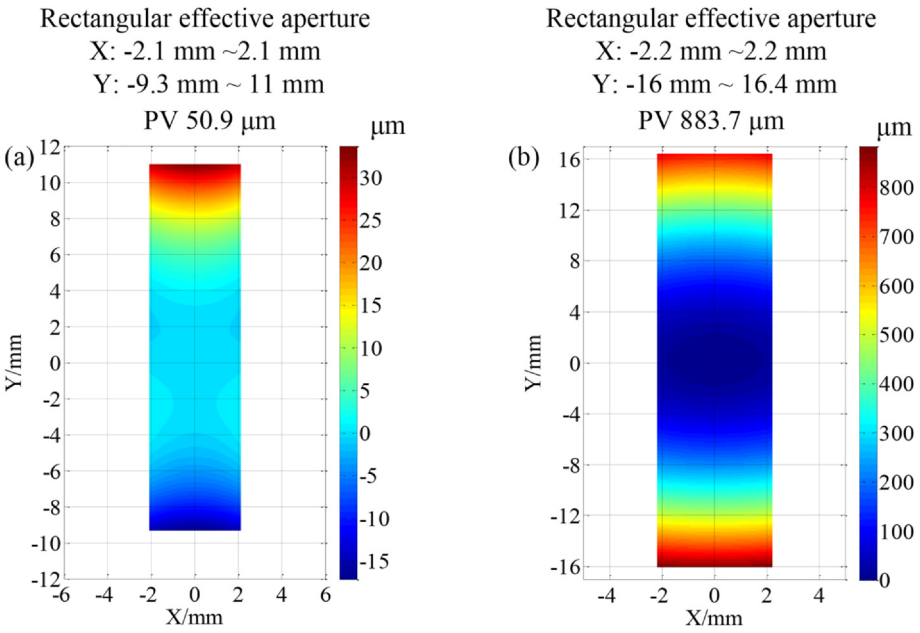

Fig. 13. Surface sag of the optimized freeform mirrors. (a) Reflective corrector, (b) primary mirror.

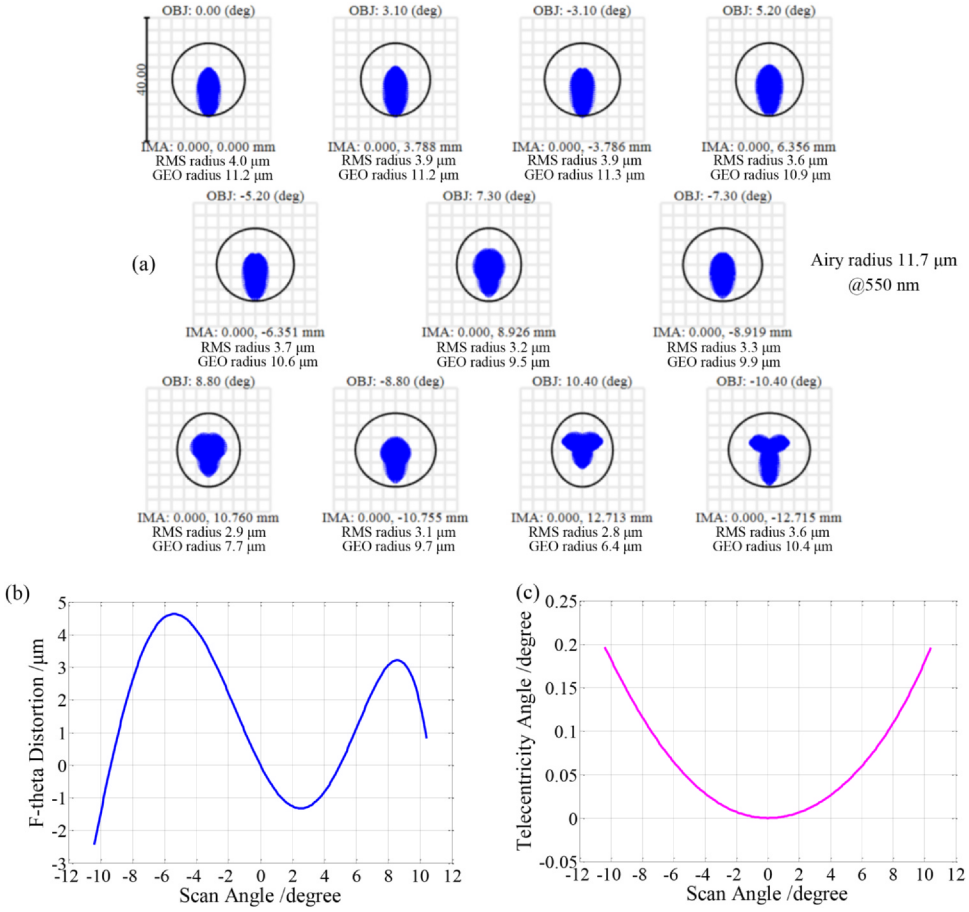

Fig. 14. Optical performance of the optimized freeform two-mirror scanning system. (a) Spot diagrams of the sampled FOVs on the image plane, (b) f-theta distortions and (c) telecentricity angles over the full FOV.

maximum f-theta distortion is within 5 μm over the full FOV as shown in Fig. 14(b), and the telecentricity angles are constrained to be less than 0.2° as shown in Fig. 14(c). The results show that an off-axis two-mirror telecentric scanning system is established, and it provides a good f-theta scanning linearity.

During the procedure of construction, the design form of the two-mirror scanning system is constrained, utilizing the freeform primary mirror for focusing function and telecentric condition realization, and

the freeform reflective corrector is adopted to fulfill the f-theta scanning geometry. This constructed configuration is critical to achieving the ultimate optical requirements, and the design concepts are maintained during the optimization process. The specifications of the two-mirror scanning system are listed in the third column of Table 1 for comparison. Other than the inherent priority of free of chromatic aberration compared with the commercial scan lens, the telecentricity is improved in the off-axis scanning system. Its working distance is 44 mm, which is shorter than that of 54 mm for the commercial scan lens, because we are not willing to employ a negative freeform mirror for surface testing and structure compactness consideration.

Conclusion

The construction method for the freeform mirrors of an off-axis telecentric scanning system with a linear FOV is depicted in detail in this paper. The feature of this scanning system is classified into focusing function, telecentric condition, and f-theta scanning geometry. A freeform primary mirror is constructed from multi OAP surfaces located at an OAP base, to fully leverage the characteristic of an OAP mirror that can focus a collimated beam or collimates a divergent source perfectly. The focusing function is fulfilled by the OAP segments corresponding to each FOV, and the telecentric condition is satisfied by the OAP base. The mapping geometry of this single mirror structure is then studied, and distortion is then found to be unavoidable because of the unsymmetrical geometry of the OAP base. Therefore, a two-mirror structure is necessary. Multiple plane mirrors are supplemented to bend the chief ray for each FOV for distortion correction. A freeform reflective corrector constructed from multiple plane surfaces located at a curved base is then adopted to fulfill the f-theta scanning geometry. Multiple plane-OAP surfaces pairs corresponding to the sampled FOVs are then expanded and mixed, to construct the freeform primary mirror and freeform reflective corrector, and the off-axis telecentric scanning system with two freeform mirrors is established. Each plane-OAP surface pair composes an ideal optical path for the specific FOV, and the freeform mirrors are constructed through these multiple surfaces expansion and mixing. Moreover, each mirror affords appropriate roles for the feature of this scanning system. The design concepts are useful for freeform system generation and optimization.

Funding

National Key Research and Development Program (2019YFB2005500); National Natural Science Foundation of China (U1931120); Foundation of key laboratory of optical system advanced manufacturing technology, Chinese Academy of Sciences (KLOMT190201); Fundamental Research Funds for the Central Universities (30919011277, 30919011278).

Declaration of Competing Interest

The authors declare that they have no known competing financial interests or personal relationships that could have appeared to influence the work reported in this paper.

References

[1] Korsch D. Anastigmatic three-mirror telescope. Appl Opt 1977;16(8):2074–7.
[2] Schiesser EM, Bauer A, Rolland JP. Effect of freeform surfaces on the volume and performance of unobscured three mirror imagers in comparison with off-axis rotationally symmetrical polynomials. Opt Express 2019;27(15):21750–65.
[3] Thompson KP, Rolland JP. Freeform optical surfaces: A revolution in imaging optical design. Opt Photon News 2012;23:32–7.
[4] Fuerschbach K, Thompson KP, Rolland JP. A new family of optical systems employing φ-polynomial surfaces. Opt Express 2011;19(22):21919–28.
[5] Zeng F, Zhang X, Zhang J, Shi G, Wu H. Optics ellipticity performance of an unobscured off-axis space telescope. Opt Express 2014;22(21):25277–85.
[6] Reimers J, Bauer A, Thompson KP, Rolland JP. Freeform spectrometer enabling increased compactness. Light Sci Appl 2017;6(7):e17026.
[7] Bauer A, Schiesser EM, Rolland JP. Starting geometry creation and design method for freeform optics. Nat Commun 2018;9(1):1756.
[8] Wassermann GD, Wolf E. On the theory of aplanatic aspheric systems. Proc Phys Soc B 1949;62(1):2–8.
[9] Bloor MIG, Wilson MJ. Using partial differential equations to generate free-form surfaces. Comput Aided Des 1990;22(4):202–12.
[10] Cheng D, Wang Y, Hua H. Free form optical system design with differential equations. Proc SPIE 2010;7849(2):78490Q.
[11] Miñano JC, Benítez P, Lin W, Infante J, Muñoz F, Santamaría A. An application of the SMS method for imaging designs. Opt Express 2009;17(26):24036–44.
[12] Duerr F, Benítez P, Miñano JC, Meuret Y, Thienpont H. Analytic free-form lens design in 3D: coupling three ray sets using two lens surfaces. Opt Express 2012;20(10):10839–46.
[13] Yang T, Zhu J, Wu X, Jin G. Direct design of freeform surfaces and freeform imaging systems with a point-by-point three-dimensional construction-iteration method. Opt Express 2015;23(8):10233–46.
[14] Yang T, Jin GF, Zhu J. Automated design of freeform imaging systems. Light Sci Appl 2017;6(10):e17081.
[15] Hou W, Zhu J, Yang T, Jin G. Construction method through forward and reverse ray tracing for a design of ultra-wide linear field-of-view off-axis freeform imaging systems. J Opt 2015;17:055603.
[16] Tang R, Zhang B, Jin G, Zhu J. Multiple surface expansion method for design of freeform imaging systems. Opt Express 2018;26(3):2983–94.
[17] Chen L, Gao Z, Ye J, Cao X, Xu N, Yuan Q. Construction method through multiple off-axis parabolic surfaces expansion and mixing to design an easy-aligned freeform spectrometer. Opt Express 2019;27(18):25994–6013.
[18] Liu J, Benítez P, Miñano JC. Single freeform surface imaging design with unconstrained object to image mapping. Opt Express 2014;22(25):30538–46.
[19] Zhu J, Yang T, Jin G. Design method of surface contour for a freeform lens with wide linear field-of-view. Opt Express 2013;21(22):26080–92.
[20] Yang T, Zhu J, Jin G. Design of freeform imaging systems with linear field-of-view using a construction and iteration process. Opt Express 2014;22(3):3362–74.
[21] Zhu J, Wu X, Yang T, Jin G. Generating optical freeform surfaces considering both coordinates and normal of discrete data points. J Opt Soc Am A: 2014;31(11):2401–8.